Energy Conversion and Management 244 (2021) 114487

Contents lists available at ScienceDirect

Energy Conversion and Management

journal homepage: www.elsevier.com/locate/enconman

Conformal heat energy harvester on Steam4 pipelines for powering IoT sensors

Kazuaki Yazawa [a,*], Yining Feng [b], Na Lu [b]

[a] Birck Nanotechnology Center, Purdue University, United States
[b] Lyles School of Civil Engineering, Purdue University, United States

ARTICLE INFO

Keywords:
Internet of things
Monitoring system
Steampipe
Thermoelectric
Energy harvesting
Analytic optimization

ABSTRACT

This paper discusses a novel design and analysis of a conformal thermoelectric generator (cTEG), which can be used for powering the internet-of-things (IoT) wireless sensors for continuous monitoring of steam pipelines operation and maintenance. This conformal device is designed to be directly attached to a cylindrical steam pipe, therefore has a mechanical flexibility to bending align to the pipe curvature (conformality), and which transports superheated steam at 200 °C or around. Lack of continuous monitoring of underground pipelines have resulted in a significant loss of money, time, and resources. This primarily is due to limited access for reading data or replacing batteries. This issue can be addressed using cTEG which can directly convert wasted heat from pipeline to electricity for continuous powering of IoT sensors. The cTEG can be made from a classical bulk bismuth telluride (Bi_2Te_3) for sintered TEG legs. In the analysis, the material properties of the legs are expected be constant and independent to the temperature where the figure-of-merit is near 1.0 at room temperature. A roll-to-roll thermoelectric module is considered by using Kapton film as the substrates with PDMS for filling the gap to achieving low cost and high performance. The electro-thermal device optimization was conducted by using analytical model. Available heat flow in the system is determined by the device design and the hot and cold side heat exchange. Hence these heat transfer limit the power output per device footprint. The moderate passive air convection can be enhanced by extending surface areas by fins to improve the power output. This work particularly focused on the optimization of the module design while the thickness is limited by the requirement of maintaining the mechanical conformability to a pipe surface. Variational conditions (steam temperature, flow rate, pipe diameter) and design parameters (fill factor and leg length) were investigated. In addition, this approach can be applied to other TEG designs with such dimension limitations. The upper limit of power output per device footprint is found at 19.5 W/m^2 with fill factor of 20%, where cTEG could achieve to 35 W/m^2 at the optimum with few centimeters thickness. The material cost to manufacture the cTEG was estimated and was found to be closer to a comparable range of the first set of primary batteries. The novel modeling method presented here can also be applied to other energy-related fields, such as geothermal, deep sea monitoring field in which heat and electricity co-optimization is of vital importance.

1. Introduction

Continuous health monitoring of the steam pipelines (for 200℃ or above superheated steam transportation) became available through wireless network internet of things (IoT) technologies [1]. Steam pipelines are critical for the heating needs od district heating [2] in populated cities in colder regions of the United States and northern part of Eurasia continent. The steam network connects 2,000 buildings for more than 105 miles of underground steam pipes, just in New York City alone [1] as an example. Preventing failure of the pipeline is significant for both cost effective maintenance and reliability for the security of city life, which is very much so as natural gas line and some other pipelines. The maintenance of pipeline IoT sensor network is challenging since many portions of the pipelines are with difficult access for battery replacement. A uniqueness for the steam pipeline is to transport heat energy, hence a fraction of the dissipated energy could be immediately converted to electricity to power IoT electronics at any unreachable locations of the pipeline.

IoT health monitoring sensors [2] are emerging technology for the pipeline failure prevention [3]. The sensors may include temperature,

* Corresponding author at: 1205 W State Street, West Lafayette, IN 47906, United States.
E-mail address: kyazawa@purdue.edu (K. Yazawa).

https://doi.org/10.1016/j.enconman.2021.114487
Received 14 April 2021; Accepted 28 June 2021
Available online 9 July 2021

pressure, flow rate fluctuation, acoustic emission [4 5], and localized strain, which are operated with wireless communication electronics to timely report the pipeline conditions. Such time-dependent information is critical to maintain the long-term reliability and to prevent from a tragic failure such as stream explosion in New York City in 2007 [6]. These IoT sensors require a power source. However, it is not cost effective to add a power line all along the underground pipeline. Or, replacing batteries every few years for all monitoring points is also unrealistic.

We investigated the potential performance of thermo-electric energy conversion for locally harvesting heat energy from the steam with analytic modeling. We analyzed if this approach can generator sufficient power to support the local IoT sensors. The simplest structure of the thermoelectric power generator (TEG) is a single piece of the thermoelectric leg (either p-type or n-type) contacting on the pipe surface as the hot side. Another side of the leg is exposed to ambient air to reject the heat via natural air convection and radiation. The thermoelectric leg is considered to be made from well-known classical bismuth telluride (Bi_2Te_3) in practice [7]. We considered that the leg is formed by sintering the small particles of the material. In harvesting heat energy to convert electricity for IoT utilization, heat sources most likely be a fluid, such as hot gas, hot water, fossil oil, steam, etc. Therefore, the pipe exterior wall surface is a key geometry to consider to recover the heat with thermoelectrics. As one of the examples, we investigated the design of conformal TEG (cTEG) module directly attached to cylindrical steam pipeline. The importance of this mechanically "conformal" feature is to minimize the thermal contact conductance through the interface. The larger the conductance, the more we have the heat that is the source of power per unit area. Especially for a case of small temperature gradient across thermal path, this is critical. The cTEG has a moderate mechanical flexibility, called bendable, so that the contact face aligns to the heat source surface such as cylinder pipes. This conformability also could work well for retrofitting to many existing pipelines. However, we do not use polymer-based flexible thermoelectric materials, which may be conducting polymer, organic/inorganic hybrids, or continuous inorganic films [8]. Among them, PEDOT:PSS are well studies such as [9] or other conducting polymers [10] have been investigated. Instead, we chose classical bismuth telluride (Bi_2Te_3), which is yet the best performance material available in market in our knowledge despite the large number of research on polymer-based flexible thermoelectric materials have been conducted. Although the advantage of polymer is its low thermal conductivity in range of 0.5 W/(m.K) or lower, the thickness is still required for the maximum power output is in centimeter range. This happens because of the low heat flux available in the system. We conducted systematic study of a variation of design parameters through the simulation based on our own analytic model to determining the optimum design with conformal structure. This paper focuses on analytical modeling and optimization in such unique conditions of IoT sensor powering on pipelines.

2. Design and configuration of thin-film thermoelectric modules

2.1. Steam pipe configuration and dimensions

Typically, the size of a branch pipe for the steam line supply to the buildings is in rage of 6–12 in. (0.15–0.3 m) in diameter. In this study, the 6 in. pipe is considered placed in a tight space where the cross section is 1 m height and 1 m width. The air temperature in the space is always at 27 °C as the thermal ground (cold thermal bath). This number is relatively conservative while the soil temperature at 50 cm deep in seasonable average is around 14.2 °C (data point location: Central Park, NY, NY) [11].

Fig. 1 highlights the heat energy flow across the cTEG. Note that usually the pipe surface area is thermally insulated except the location where the cTEG is utilized. Fig. 2 shows the schematic of the bendable feature of cTEG modules.

2.2. Material properties of cTEG design

We set the design of cTEG module with 40 pairs n- and p-type legs on a 40 mm × 40 mm area. Above Fig. 2 shows the structure of the module, which looks similar to an off-the-shelf solid TE module but mechanically flexible. To be fair, we assumed a TE materials Bi_2Te_3 with mean zT value of 0.85 at the mean operation temperature. For our analysis with the theoretical model, we picked a set of dimensions and material properties. The dimensions of the n- and p-type TE legs are 1 mm × 1

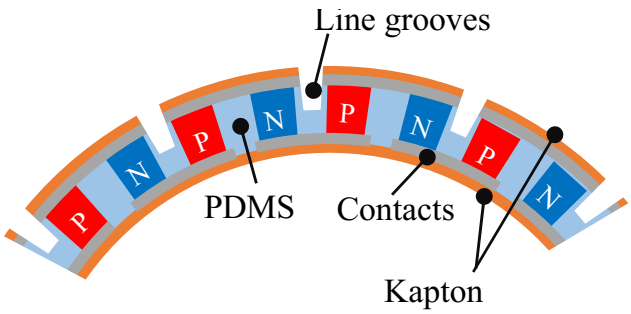

Fig. 2. Cross section of bendable cTEG module. Line grooves allow the larger streach of the outer liner for bending to fit to the pipe surface.

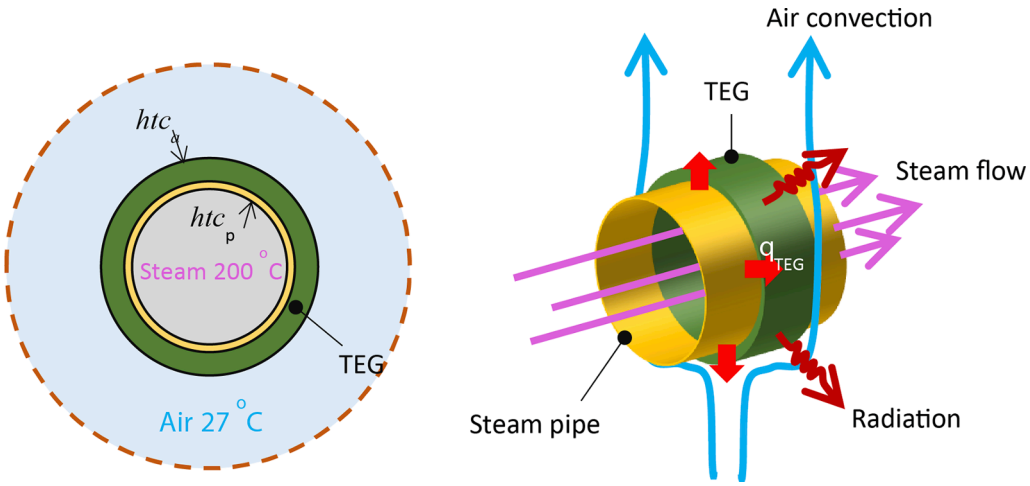

Fig. 1. Heat transfer component of the steam pipe application.

mm and variable height. Kapton in thickness of 273 μm is used for the substrates found from commercial product, which is a thermally conductive and electrically insulating polyimide film. The thermal conductivity is 1.76 W/(m.K) at 300 K drawn from ref [12]. The gaps between the legs must be filled with a flexible material to achieve the mechanical conformability. We chose PDMS for the gap fill. See Ref [13] for the impact of gap fill thermal conductivity. The thermal conductivity of PDMS is set to 0.15 W/(m.K) in entire operation temperature range. Since PDMS is an insulating material, no passivation layer between the above metal layer is considered. The benefit of using a gap fill material is that radiation thermal cross talk between the hot and cold interim walls is completely eliminated. In this analysis, we also assumed a 30 μm thick metallization pattern for the interconnects with electrical conductivity of $6x10^7$ [S/m].

3. Electro-thermal optimization

The model considers a single piece of thermoelectric leg, and it assumes a uniform array of p-type and n-type junctions with the same property values except the polarity of Seebeck coefficient. All material properties take the average value from temperature dependency. By formulating from energy balance equations, the maximum power output is found from true external boundary conditions (steam and air). We are dealing with an enormously large heat mass of the steam, e.g., supplying 37.8 kW of heat per pipe (taking into account the latent heat alone) with 0.19 kg/s of flow rate, where the power needed for IoT sensor is only a few 100 s mW for each. Hence, the energy conversion efficiency does not matter, while maximizing power output per device is important, which is directly related to the cost.

3.1. Heat transfer components across the system

Heat transfer components are investigated and modeled with using selected empirical correlations. The heat source is a super-heated steam flow with the fixed temperature of 200 °C, which is the hot side temperature reservoir. This means that the temperature of steam will change negligibly small when it flows through the section heat energy harvesting. This is a reasonable assumption as long as the sensible heat supplied by the steam flow is significantly large compared to the heat extracted for the local power generator(s). Where, no phase change should occur. The cold side temperature reservoir is defined by the ambient temperature 27 °C of air via passive convection or surrounding wall(s) via radiation heat transport. In order to allow the natural convection with gravity effect, a sufficient surrounding space is assumed for the suspended steam pipe.

Fig. 3 is the overall system diagram with a thermal resistance network in conjunction with an electrical circuit. However, for simplification, the diagram contains single leg. In the real modules, the legs are connected electrically in series and thermally in parallel. The electrical current flow and the heat flow deeply interplay each other, hence these effects cannot be separately analyzed. In the figure, ψ_h and $\psi_c$are the thermal resistances for the heat transfer on the hot side and cold side, respectively. The resistance network modeling and the design optimization of the core part of TEGs is detailed in previous work [9].

The power output per unit area w [W/m^2] by knowing T_h and T_c is

$$w = \frac{m\sigma S^2}{(1+m)^2 d}(T_h - T_c)^2 \tag{1}$$

where m is electrical load resistance ratio $m = R_L/R$, σ is electrical conductivity $[S/m]$, S is Seebeck coefficient [V/K], and d [m] is the length of the thermoelectric legs. If this d is very large, power output diminishes where the temperature difference $(T_h - T_c)$ cannot exceed the entire temperature difference of the system boundary $(T_s - T_a)$. On the other hand, if d is very small, the temperature difference $(T_h - T_c)$ becomes very small. Hence there should be the optimum d to maximize

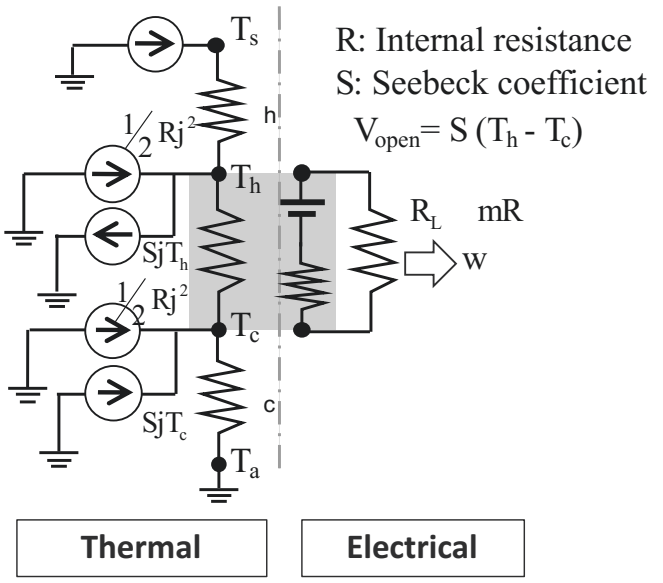

Fig. 3. Electro-thermal resistance network model. The center hatch represents a chunk of thermoelectric material (leg) and the upper and lower nodes of the region represent the electrical and thermal contacts.

the power output.

$$d_{optimum} = km(\psi_h + \psi_c) \tag{2}$$

where k [W/(m.K)] is thermal conductivity and ψ_h, ψ_c [m^2.K/W] are thermal resistances of the hot and cold side of the legs. These two temperatures depend on the thermal resistance as well as the electrical heat generation internal of electrical circuit as mentioned above. Hence both electrical and thermal optimization must be performed simultaneously. Since we already know that happens at the following condition in the electrical circuit, the R_L is considered always matched to the optimum. Then,

$$m = \sqrt{1 + Z\overline{T}} \tag{3}$$

where, $\overline{T}$is the operation temperature $\overline{T} = (T_h + T_c)/2$ and Z is figure of merit of the thermoelectric material.$Z = \sigma S^2/k$.

The analytical maximum power output per unit area is found by knowing both the hot and cold side temperature of the leg.

$$w_{maximum} = \frac{mZ}{(1+m)^2}\frac{k}{d_{optimum}}(T_h - T_c)^2 \tag{4}$$

From the given boundary temperature by knowing optimum parameter $d_{optimum}$, the maximum power output is found as the following. The detail of formulation is found in Ref. [14].

$$w_{maximum} = \frac{mZ}{\alpha^2(1+m)^2}\frac{k}{d_{optimum}}(T_s - T_a)^2 \tag{5}$$

where α is the factor determined by the external thermal resistances and internal thermal resistance of the legs. Typically, this value is near 2 as both the hot and cold thermal resistances are similar.

In the process of finding optimum design: $d_{optimum}$, $T_{h,}$ and T_c are still involved in the equation. Iterative calculation has been conducted with giving fill factor and number of legs per unit area to obtain the solution. We already know that there is only one global optimum point exist across the entire variation of leg length d. Also, the power output tends to be insensitive to the parameter change near at the peak. Hence a very simple algorism is applied, see Fig. 4.

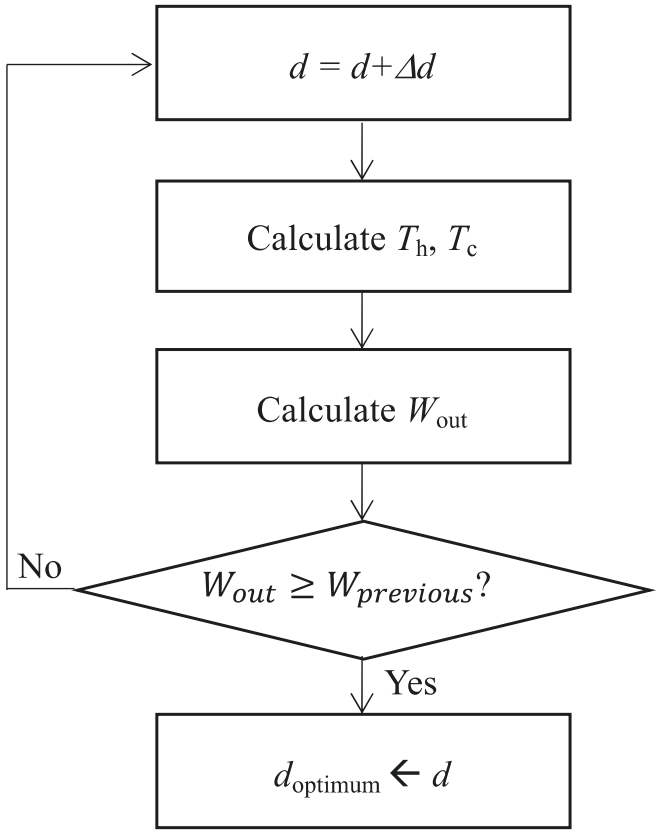

Fig. 4. Flow chart of the design optimization process.

3.1.1. Convection inside of a circular pipe

Internal heat transfer from the steam (200 °C) to the interim wall surface of a 6-inch diameter steam pipe was determined by utilizing Sieder and Tate correlation [15] for fully developed turbulent flow. This correlation includes the temperature gradient of bulk flow and nearby wall to reflect the temperature dependency of the fluid property.

$$Nu_D = 0.027 {Re_D}^{4/5} Pr^{1/3} \left(\frac{\mu}{\mu_w}\right)^{0.14} \quad \{\text{valid for } Re_D > 10,000\} \tag{6}$$

where subscript D stands for the pipe diameter, μ is bulk viscosity and μ_w is that at near wall.

The flowrate of steam is taken into account its temperature-dependent and pressure-dependent specific heat and viscosity. Considering a heating capacity of 37.8 kW of an underground pipe line with the steam, the mass-flowrate of 0.19 kg/s is required, where Reynolds number is $Re_D > 1.03 \times 10^5$ with bulk velocity of 22 m/s. Along the pipeline, convection between the bulk steam flow and the interim wall of the pipe is a function of total heat loss through the pipe exterior. Typically, the pipe is covered by a thermal insulator. A fraction of exterior is used for the thermal energy harvester. Hence the steam flow is considered as temperature reservoir. The heat flow Q by steam is simply determined by the sensible heat brought to the ideal condenser at saturate temperature T_{sat} as

$$Q = \rho u A C_p (T_{steam} - T_{sat}) \tag{7}$$

where $u = \mu Re_D/(\rho D)$. Here, the bulk velocity u is determined. Then, the Reynolds number is plugged-in to Eq. (6) to find the heat transfer coefficient as

$$htc_p = k_f Nu_D / D \tag{8}$$

Under the condition stated above, Nusselt number Nu_D is 261 and then heat transfer coefficient is 55 W/(m^2.K).

3.1.2. Natural convection and radiation heat rejection from exterior of a circular pipe

The heat transfer from the exterior of the pipe to the ambient is calculated based on passive air convection and the radiation heat transport to the surrounding walls. The model considers only the section of pipeline where the thermoelectric power generator is applied. We used the correlation by Churchill and Chu [16] for the air convection from an infinitely long horizontal cylinder to ambient, where the cylinder is suspended in the air with no thermal contact. The surrounding space is assumed to be sufficiently large so that airflow induced by buoyancy will not be disturbed. The Nusselt number is found as

$$Nu_D = \left\{ 0.60 + \frac{0.387 {Ra_D}^{1/6}}{\left[1 + (0.559/Pr)^{9/16}\right]^{8/27}} \right\}^2 \tag{9}$$

where the diameter-basis Rayleigh number Ra_D is found as

$$Ra_D = \frac{g\beta(T_c - T_a)D^3}{\nu\alpha} \tag{10}$$

where g is gravity, β is coefficient of thermal expansion, ν is viscosity and α is thermal diffusivity. The non-linear radiation heat transfer takes effect in a same order of natural convection when the convection is weak even at the temperature excess of the surface is as high as 10 s degrees. In this model a gray body thermal emission is considered from the pipe surface with emissivity value of 0.85 (oxidized and untreated). The surroundings are considered infinitely far from the pipe compared to the pipe diameter, so that far infrared wavelength reflection coming back from the surrounding wall is minimal and neglected. In this case, one-way heat removal by radiation is considered.

$$htc_{a\_eff} = \frac{k_f}{D} Nu_D + \sigma\varepsilon\left({T_c}^4 - {T_a}^4\right)/(T_c - T_a) \tag{11}$$

where k_f is thermal conductivity of air, σ is Stefan-Boltzmann constant, and ε is emissivity of the pipe surface.

By integrating the above with thermoelectric generator model, the Fig. 5 shows the contribution of the hot and cold side heat transfer in a system (see Fig. 6).

3.2. Electro-thermal optimization

In this application, we focus on maximizing the power output per

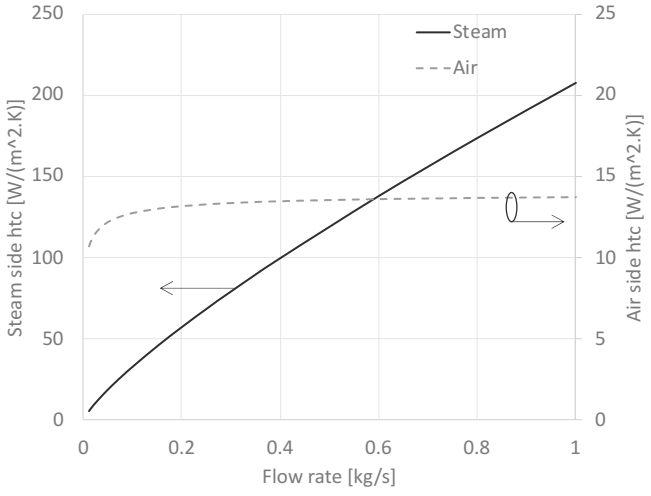

Fig. 5. Heat transfer coefficient values calculated for the steam and air sides as the functions of flow rate. The flowrate makes some changes on cold side heat transfer in very small range, where the steam mass flow rather dominates the system thermal resistance.

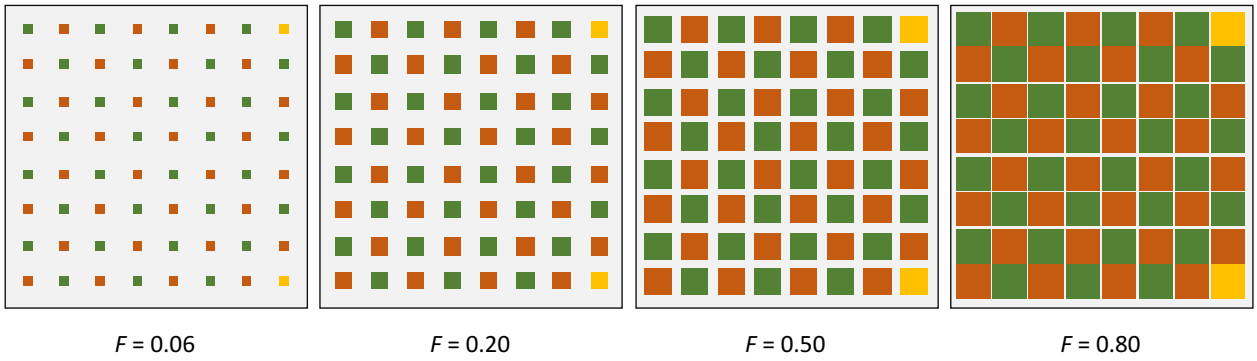

Fig. 6. Example of thermoelectric 8 × 8 legs in checkerboard layout on a rectangular substrate with varying the fill factor (0.06, 0.20, 0.50, 0.80). The n-type and p-type legs are located next each other like a checkerboard. Right two corners are reserved for wire terminals so that total number of legs is 62.

given dimension. To this end, calculation is based on the temperature independent material properties: thermal conductivity of 1.07 W/(m.K), electrical conductivity of 58,750 (1/Ω.m), and Seebeck coefficient of 191 μV/K. The material zT value is 0.85. As the property profile changes a lot by changing doping level or the processes, we do not use temperature dependent properties in this work [17].

The temperatures at the hot and cold side of the module obviously not equal to the boundary temperatures (steam temperature of 200 °C and ambient temperature of 27 °C), which are temperature reservoir (or thermal bath). Depending on the internal and external thermal resistances, the heat flow cross the legs is determined. Hence the actual temperature at the terminals of the thermoelectric leg is determined by the thermal diffusion as well as the additional heat flow induced by allowing electrical current flow across the legs. It is necessary to co-optimize with electrical and thermal energy transports as both of them are interdependent.

3.3. Design optimization with leg length limit

The key factors of thermoelectric module are the fill factor F (fractional area coverage of thermoelectric leg), the leg length d, and the number of legs per unit area N. Design optimization was conducted with focusing on the impact of fill factor and leg length with coordinating the manufacturing process. It is known that the power output per unit area is independent to N as long as d and F are kept constant. Hence, we investigated the impact of leg length and fill factor. Following figure visualize how the TE elements occupy the footprint by varying fill factor. The calculations were conducted in a wide range from 0.02 (2%) to 0.99 (99%).

In this particular application, some level of mechanical flexibility is required to the module to fit to the curvature of the cylinder pipe surface. The flexible module may not be thicker than 10 mm or so since we assumed the pipe diameter of 6 in. (~150 mm) as the benchmark. We set a maximum module thickness of 5 mm as the threshold of evaluation, which means that the maximum allowable the leg length is 5 mm.

Fig. 7 shows the maximum power output and the optimum fill factor while the leg length is the design variable. No heat transfer enhancement on the cold side is considered. At the maximum power output condition, the relationship between the leg length and fill factor is proportional.

3.4. Heat transfer enhancement for air cooling side

Based on the given conditions, the cold-side external thermal resistance dominates the net thermal resistance across the system ($htc_a < htc_p$). If a larger thermal harvesting is desired, the heat flow through the generator is easily enhanced by reducing the cold side thermal resistance as long as the generator is optimally designed. In practice, enhancement of natural convection is the primary challenge for the improvement. We investigated a pin–fin heat transfer enhancement

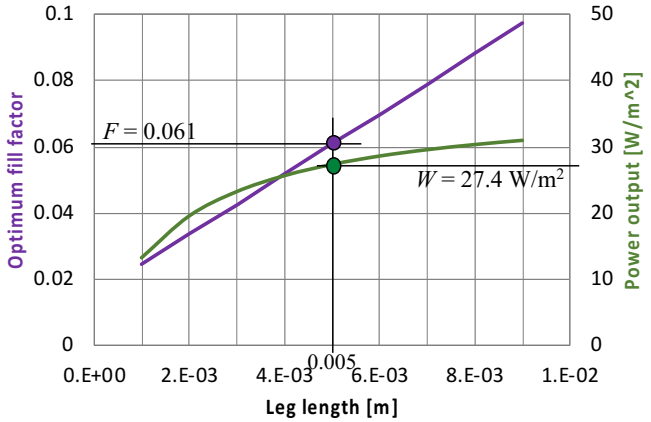

Fig. 7. Power output and optimum fill factor as the functions of leg length with no heat transfer enhancement on the cold side.

on the cold-side passive air convection in the analysis. We used the Aihara's correlation [18] for circular pin-fins in the calculation. The heat transfer is found using Rayleigh number Ra^* based on the horizontal pin spacing $S_h$is found as

$$Ra^* = \frac{Prg\beta(T_w - T_a)s_h^4}{H\nu^2} \tag{12}$$

where g is gravity, β is coefficient of thermal expansion, ν is viscosity, and H is the effective vertical length of pin–fin array. Then, the Nusselt number with pin–fin array is described as

$$\left(\frac{\pi d_p}{2s_v}\right)Nu_p = \frac{Ra^{*3/4}}{20}\left[1 - e^{-\frac{120}{Ra^*}}\right]^{1/2} + \frac{Ra^{*1/4}}{200} \tag{13}$$

where d_p is diameter of circular pin–fin, and $S_h$is vertical pin spacing. The heat transfer coefficient is then found as

$$htc_{pin} = Nu_p\frac{k_f}{s_h} \tag{14}$$

The pin–fin enhancement allows the improvement from13.9 W/(m^2.K) to 17.4 W/(m^2.K) in heat transfer coefficient. The impact of this heat transfer for the design is shown in the Fig. 8.

Theoretical maximum power output with an ideal module design shows a potential up to 48 W/m^2 range, where the optimum leg length is significantly large for the larger fill factor as seen in Fig. 7. In a realistic design, however, one must choose a design point, which is off the maximum power with shorter leg length than the optimum. That is because the limitation of the length by mechanical flexibility of the

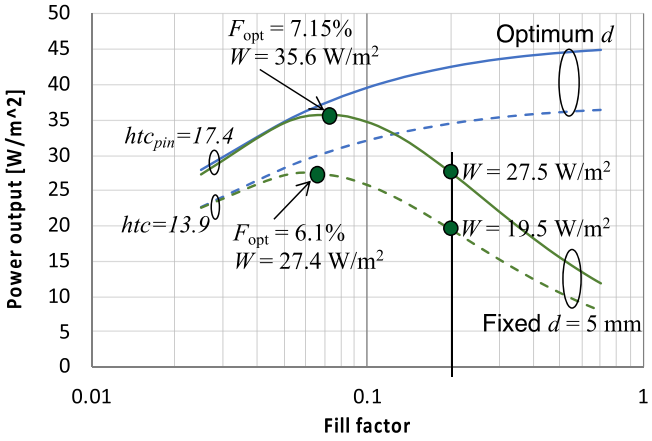

Fig. 8. Power output as function of fill factor for the cases of fixed leg length (5 mm) and variable leg length optimum for the maximum power output. The dotted curves show untreated surface, and the solid curve shows the case with a pin–fin enhancement.

module ($d \leq 5mm$). The Fig. 8 shows the power output as function of fill factor with fixed and optimized leg length. From manufacturing standpoint, too small fill factor makes a significant challenge to secure the electrical and thermal contacts. In our assumption, the fill factor of 0.2 would be the good range of practice (see Figs. 9–12).

The performance of the thermoelectric module in practice was estimated to generate 19.5 W/m^2 with thickness of 5 mm and the fill factor of 0.2, according to the material properties and heat transfer conditions. This translates that the power harvesting with a 6-inch diameter steam pipe is more than 40 W/m of power output per pipe length. To make the IoT sensors work, only a few cm of width will be sufficient. Or utilizing a quarter circumference of the pipe with less than 10 cm width will be enough to charge the IoT sensors.

3.5. Impact of design and operation conditions

3.5.1. Pipe diameter

Pipe diameter may vary depending on the conditions of pipeline. The steam flowrate likely relates to the diameter per design. However, the flowrate is fixed to 4 kg/s in this analysis to see pure impact of the flow velocity on the heat transfer. Obviously, velocity is lower in larger pipe,

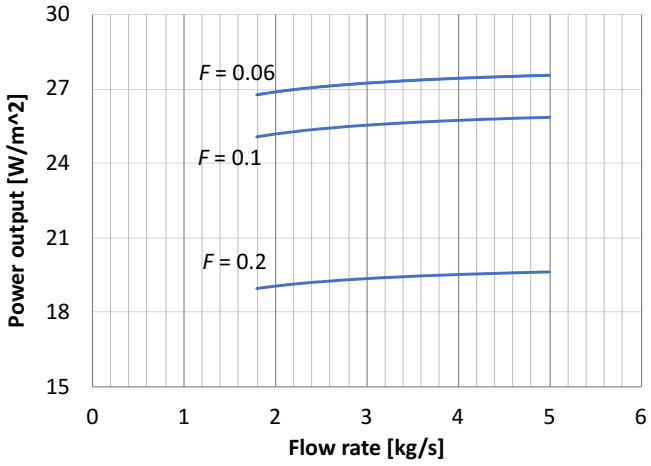

Fig. 10. Power output vs Flow rate. This is a case of the fixed leg length 5 mm.

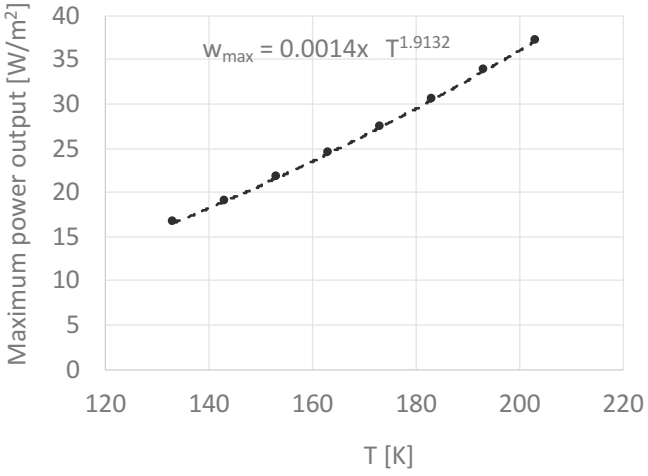

Fig. 11. Maximum power output as function of temperature difference (ΔT) between the steam and ambient air (26.85 °C) while TE leg length is constrained. The dots are calculation results with an exponential curve fitted. The trend is nearly proportional to the square of ΔT.

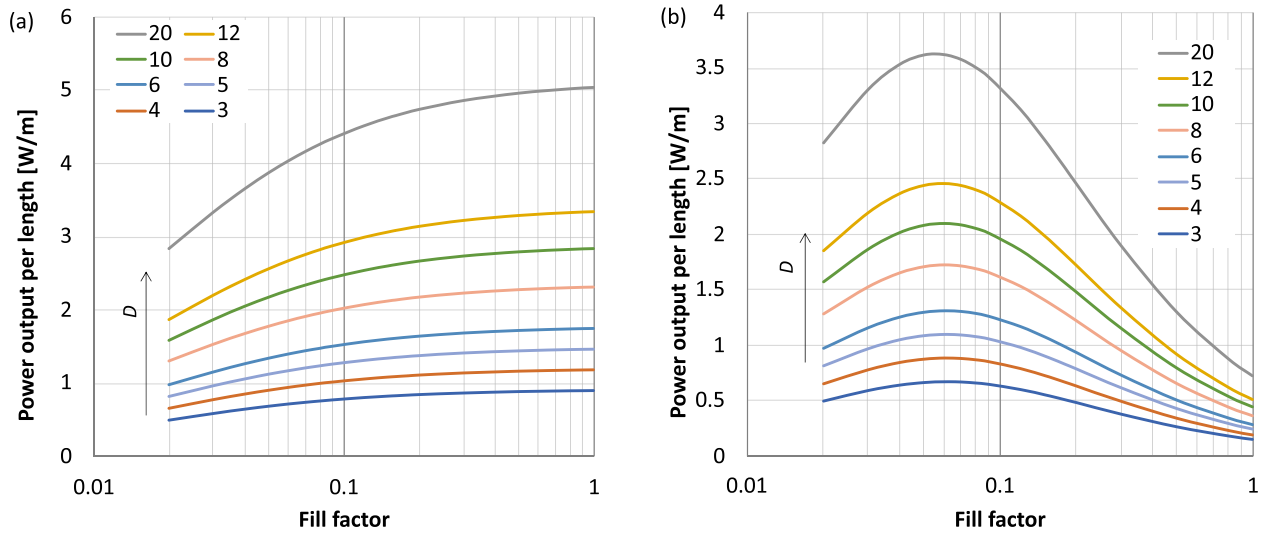

Fig. 9. Power output as function of fill factor with varying pipe diameter from 3 in. (7.6 cm) to 20 in. (50.8 cm). (a) shows the case thickness of the module is not limited and (b) shows the case leg thickness is fixed to 5 mm as previous analysis. The Power output is measured per unit pipe length [W/m], where TE module is applied to the entire circumfarence of the pipe cross section.

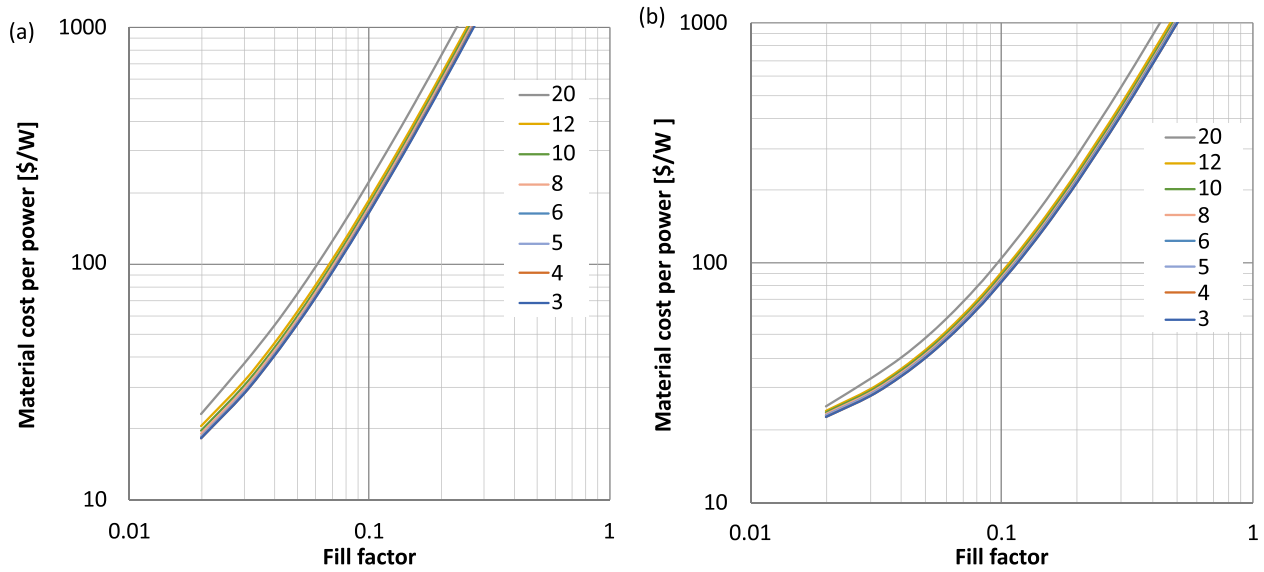

Fig. 12. Material cost per power output [$/W] as a function of fill factor in variation of pipe diameter in inch. (a) shows the case without limiting the leg length and (b) shows the case with fixed leg length $d = 5$ mm. Material prices are $500/kg with density of 8200 kg/m^3, $5/kg with density of 965 kg/m^3, and $175/kg with density of 1420 kg/m^3 for Bi_2Te_3, PDMS, and Kapton, respectively.

but the surface area is larger. As the result, extension of surface area by extended pipe diameter increases the capacity of power output as a system.

3.5.2. Flow rate

In other direction of designing the pipeline, varying the steam flow rate is another parameter. Or, in real operation, it may unintentionally vary. In unlimited TE leg length, a larger power output per unit pipe length is observed at increased flow rate within the evaluated range (2 – 5 kg/s). However, the power output per unit area by controlling the leg thickness ($d = 5$ mm), the change by changing flow rate is almost negligible.

3.5.3. Steam temperature

The steam temperature may change under the control, by incident, or due to a potential failure of the system. Power generation is in general near proportional to the square of the temperature difference. Hence the power output is a good indicator of health monitoring steam distribution. Folloing components are affected by the steam temperature.

(1) Steam side: If steam temperature is sufficiently larger than saturation temperature ($T_{\text{steam}} > T_{\text{sat}}$), convective heat transfer linearly changes by the temperature difference ($T_{steam} - T_{wall}$). The saturation temperature plays a significant role where the latent heat involved, and it becomes nonlinear.
(2) Air side: There are two components. One is convection term, where heat transfer changes roughly by $(T_c - T_{air})^{2/3}$. And radiation heat transfer changes roughly by $(T_c - T_{air})^4$
(3) TE device: The power output changes by $(T_h - T_c)^2$.

Obviously, all components link together. If design is conducted for each temperature condition, the maximum power output in overall will approximately change by $(T_h - T_c)^2$ and then it will be approximately proportional to $(T_{steam} - T_a)^2$ without considering the thickness restriction for mechanical flexibility.

3.6. 3D simulation

Extended work with full 3D computational fluid dynamic (CFD) modeling has been conducted on a commercial software package; ANSYS FLUENT. Unfortunately, we could not obtain the results for direct comparison with analytical modeling due to a fundamental challenge.

The major difficulty with 3D CFD with this problem is the large difference between internal pipe flow (turbulent, fully developed flow) and external convection flow (laminar, developing flow). Therefore, convergency of solution tends to be driven by turbulent parameters, which are the turbulent kinetic energy (k) and the rate of dissipation of it (ε) in our choice of turbulent viscos flow model so called k- ε model with Re-Normalization Group (RNG) method. Mitigating this challenge by separating the calculation domains in parallel does not work in this special case, since we have energy conversion device in the middle. Then, the distribution of heat flux across the device makes a quite large impact to the performance. Heat flux changes the electrical load voltage and then change the effective internal distributed thermal resistances. We will keep pursue the method in future to overcome this challenge in 3D numerical simulation for a thermoelectric power generator system.

3.7. Cost impact

Fill factor makes a significance influence on the cost to build the cTEG module since the thermal impedance matching with the external contacts is the key to find the maximum power output per unit area. Following figure shows the material cost per unit power output as a function of fill factor, where the impact of fill factor is significant. The figure also shows the variation of the pipe diameter. The diameter shows a moderate impact to the cost. Interestingly, the cost for power is lower for the fixed length (5 mm) at fill factor from around 3% and larger, compared to the design of optimum leg length. In comparing the cost performance in $/W with the primary batteries with bulk package in the market (see Table 1), only a smaller fill factor design of cTEG is potentially match the initial investment and until the battery life ends. The cost including replacement and human cost thereafter only piles up on primary batteries while thermoelectric remains to work.

3.8. Preliminary experimental results

Although this paper is on focus of analytic modeling, we have collected a preliminary data from our proof-of-concept experiments with 8 legs in a 40 mm × 40 mm module. Fig. 13 shows the power output per unit area as a function of the controlled temperature difference across

Table 1
Initial cost and energy cost of primary batteries.

Primary battery type	Power W	Initial cost $/W	Capacity Wh	Energy cost $/Wh
9V	0.13	8.96	0.57	2.05
AAA	0.03	7.33	1.15	0.19
AA	0.03	8.33	2.87	0.09
C	0.06	28.08	7.8	0.21
D	0.06	36.75	17	0.12

Note: The prices were the minimum price found from Amazon.com [19] as the date of investigation June 9, 2021, and do not necessarily represent the shipping price from the manufacturers. Other technical information is from [20].

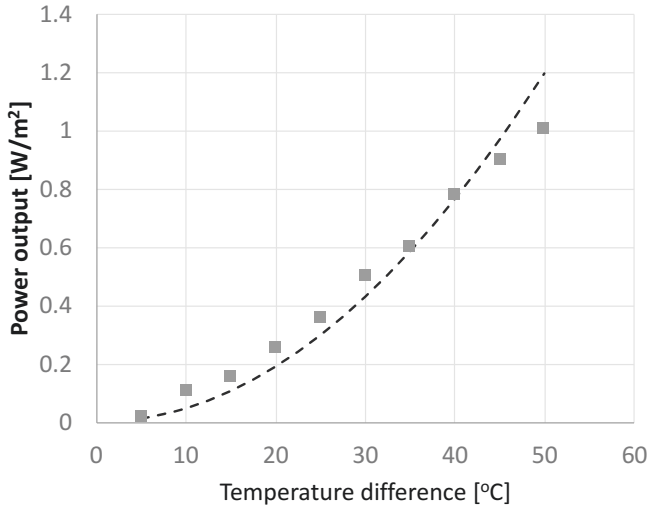

Fig. 13. Power output per unit area vs temperature difference across the cTEG module. Dots are experimental data and broken curve is the model based on the effective properties extracted from the experiments. The dots follow the trend of ΔT^2.

the cTEG module compared with Eq. (1). The dots are experimental data, and the broken curve is the theoretical result with the effective dimensionless figure of merit $zT = 4.03\text{x}10^{-2}$ at room temperature. This zT value is significantly smaller compared to a known typical value of Bi_2Te_3 because of the large contact resistances with premature process as well as the large heat loss through the PDMS gap fill at the moment. The leg dimensions are 0.5 mm × 0.5 mm and 3.5 mm in cross section and length, respectively.

4. Conclusions

In this study, we have proposed and systematically examined a new method for the design and analysis of conformal thermoelectric generator (cTEG) that can be installed on steam pipelines for powering IoT monitoring sensors. To realize a cost-effective and practical manufacturing process based on roll-to-roll platform, Kapton film substrates with PDMS support for the classical Bi_2Te_3 materials are investigated. The electro-thermal device optimization was conducted by using an analytical model. The heat transport boundaries of the module are modeled with the combination of heat transport correlations. On the hot side, convective heat transport from the 200 °C steam to the interim wall of the pipe. On the other side, passive air convection and radiation heat removal to the tunnel wall were defined on the exterior of the cTEG module. The thickness of the thermoelectric module is a design constraint to be practically conformal to the steam pipe surface. The upper limit of the thickness depends on the material and design of the module. In this analysis, we compared the case imaginably without the thickness limit and the other case of 5 mm thick. The optimum thickness inversely larger as the capacity of heat flux by passive air convection is moderate and is much larger than a few cm in this case. In the results, the optimum fill factor was observed at aggressive number 6.5% where the power generation was 27.4 W/m^2. The power output of 19.5 W/m^2 was found with a reasonable fill factor of 20% and the thickness of 5 mm for mechanical conformability. It could reach the 35 W/m^2 range with addition of heat fins if the thermal resistance across the module could be optimized either very thick module or an order of magnitude smaller thermal conductivity of the thermoelectric material. The power and voltage output are sufficient to power IoT sensor network which are typically operating at micro-watt regime. This science developed from this work can also be used for other engineering fields of heat transfer and/or heat energy harvesting, such as the hot oil or spring water transfer, the heating and cooling water pipeline network in large commercial buildings, chilled ware supply in datacenters, etc. Variational analyses were demonstrated with varying steam temperature, flow rate, and diameter of the pipes based on the developed model for source fluid temperature. Cost estimate using industry suggested unit price of raw materials is found to be comparable in the initial cost per unit power with larger primary batter. The cTEG modules will not require further costs of replacement and the additional human work as the primary batteries do. This analysis method can help accelerate the technology adoption as the cost is often a major hinderance.

CRediT authorship contribution statement

Kazuaki Yazawa: Methodology, Formal analysis, Investigation, Writing – original draft. **Yining Feng:** Data curation, Writing – review & editing. **Na Lu:** Conceptualization, Supervision, Writing – review & editing.

Declaration of Competing Interest

The authors declare that they have no known competing financial interests or personal relationships that could have appeared to influence the work reported in this paper.

Acknowledgements

This work was supported by a research grant provide by National Science Foundation (NSF). The grant number is 1919191.

References

[1] Zhu Q, Wang R, Chen Q, Liu Y, Qin W, Iot gateway: Bridgingwireless sensor networks into internet of things, In 2010 IEEE/IFIP International Conference on Embedded and Ubiquitous Computing, pp. 347-352. IEEE, (2010).
[2] Kumar NS, Mallikharjuna RK, Kothuru M, Rao YN. Multi-dimensional parametric assessment with IoT in acquaintance of digital pipeline. Int J Electr Comput Eng 2019;9(6):4649.
[3] Giurgiutiu V, Cuc A. Embedded non-destructive evaluation for structural health monitoring, damage detection, and failure prevention. Shock and Vibration Digest 2005;37(2):83.
[4] Ozevin D, Harding J. Novel leak localization in pressurized pipeline networks using acoustic emission and geometric connectivity. Int J Press Vessels Pip 2012;92:63–9.
[5] Oh SW, Yoon D-B, Kim GJ, Bae J-H, Kim HS. Acoustic data condensation to enhance pipeline leak detection. Nucl Eng Des 2018;327:198–211.
[6] The New York Times, Steam Blast Jolts Midtown, Killing One, retrieved from https://www.nytimes.com/2007/07/19/nyregion/19explode.html.
[7] Witting IT, Chasapis TC, Ricci F, Peters M, Heinz NA, Hautier G, Snyder GJ. The thermoelectric properties of bismuth telluride. Adv Electron Mater 2019;5(6):1800904.
[8] Wang Y, Yang L, Shi X-L, Shi X, Chen L, Dargusch MS, Zou J, Chen Z-G. Flexible thermoelectric materials and generators: challenges and innovations. Adv Mater 2019;31(29):1807916.
[9] Xu S, Hong M, Shi X-L, Wang Y, Ge L, Bai Y, et al. High-performance PEDOT: PSS flexible thermoelectric materials and their devices by triple post-treatments. Chem Mater 2019;31(14):5238–44.
[10] He M, Qiu F, Lin Z. Towards high-performance polymer-based thermoelectric materials. Energy Environ Sci 2013;6(5):1352–61.

[11] Henry Mount Soil Temperature and Water Database, Natural Resources Coservation service a part of United States Department of Agriculture, User Site ID 1997NY061002, http://soilmap2-1.lawr.ucdavis.edu/henry/.
[12] Benford DJ, Powers TJ, Moseley SH. Thermal conductivity of kapton tape. Cryogenics 1999;39(1):93–5.
[13] Koh YR, Yazawa K, Shakouri A, Nagahama T, Maeda S, Isaji T, et al. Analytical optimization of the design of film-laminated thermoelectric power generators. J Electron Mater 2019;48(11):7312–9.
[14] Yazawa K, Shakouri A. Optimization of power and efficiency of thermoelectric devices with asymmetric thermal contacts. J Appl Phys 2012;111(2).
[15] Sieder EN, Tate GE. Heat transfer and pressure drop of liquids in tubes. Ind Eng Chem 1936;28(12):1429–35.
[16] Churchill SW, Chu HS. Aorrelating equations for laminar and turbulent free convection from a horizontal cylinder. Int. J. Heat Mass Transfer 1974;18:1049.
[17] CRC Handbook of Thermoelectric, Ed. D.M. Rowe, CRC Press, 1999.